Chemical Science

ROYAL SOCIETY OF CHEMISTRY

EDGE ARTICLE

View Article Online
View Journal | View Issue

Cite this: *Chem. Sci.*, 2020, **11**, 8495

All publication charges for this article have been paid for by the Royal Society of Chemistry

A ratiometric fluorescent probe for real-time monitoring of intracellular glutathione fluctuations in response to cisplatin†

Hanzhuang Liu, ‡ Wenting Song,‡ Shuren Zhang, Kin Shing Chan, Zijian Guo * and Zhen Shen *

Received 22nd May 2020
Accepted 28th July 2020

DOI: 10.1039/d0sc02889d

rsc.li/chemical-science

Real-time imaging of fluctuations in intracellular glutathione (GSH) concentrations is critical to understanding the mechanism of GSH-related cisplatin-resistance. Here, we describe a ratiometric fluorescence probe based on a reversible Michael addition reaction of GSH with the vinyl-functionalized boron-dipyrromethene (4,4-difluoro-4-bora-3*a*,4*a*-diaza-*s*-indacene or BODIPY) **1**. The probe was applied for real-time monitoring of the fluctuations in GSH levels in cells under cisplatin treatment. Notably, in cellular cisplatin-sensitive A549 cells, GSH concentrations rose until cell death, while in cisplatin-resistant cell lines, GSH levels first rose to the maximum then fell back to the initial concentration without significant apoptosis. These results indicate that different trends in GSH fluctuation can help distinguish cisplatin-resistant from cisplatin-sensitive cells. As such, this study has shown that probe **1** may potentially be used for real-time monitoring of intracellular GSH levels in response to therapeutics.

Introduction

Glutathione (GSH) is the most abundant non-protein thiol in cells and plays a critical role in maintaining intracellular redox homeostasis.[1] Alterations in glutathione levels are associated with several cellular functions and diseases,[2] including immune responses, Parkinson's disease, cancers, *etc.* GSH also plays an important role in detoxification processes by binding itself to toxins. With the help of glutathione-*S*-transferases, GSH embeds itself on toxins, flagging them as hazardous, thereby helping remove chemical substances from the cells.[3] Cisplatin is one of the most powerful divalent platinum (Pt^{II}) anticancer drugs in clinical use, but its wider application is limited by its toxicity and the resistance of some cancers. GSH has been recognized to play a major role in cisplatin resistance, since the cells resistant to cisplatin often have elevated levels of cellular GSH.[4,5] However, the role of GSH in enhanced cellular resistance to cisplatin is still under debate, since some researchers have reported that there was no correlation between the amount of GSH in the cells and the efficacy of cisplatin.[6] In order to distinguish the differences in GSH levels in cisplatin-resistant from cisplatin-sensitive cells, it is necessary to monitor the changes in GSH concentration in real time.

Fluorescent probes are promising tools for detecting GSH in living cells. The primary requirement for real-time fluorescent probes is the reversibility of the response to variations in GSH concentrations.[7] In addition to reversibility, the following key aspect should also be considered. A ratiometric probe will have to minimize artefacts that may arise from variations in excitation intensity, probe concentration, dye distribution, and the intracellular environment.[8,9] Using a significantly lower concentration (μM) of the probe to quantify millimolar levels of GSH is generally favoured to minimize cytotoxicity and disturbance on the biological system.[7,10] Additionally, both the forward and reverse reactions need to proceed rapidly because endogenous changes in GSH concentration may be completed in 1–30 minutes.[11,12] Furthermore, in order to obtain a clear fluorescence image for confocal microscopes, the fluorescence quantum yield of the probe should be high; the excitation wavelengths should match the commonly used laser wavelengths; and the shift in emission profiles upon reaction with GSH should be large.[7,13] The interference from molecules with similar reactivity and/or higher working concentrations, as well as pH must be considered and excluded.[8] Lastly, the probe should have sufficient cellular permeability and minimal toxicity.

A number of fluorescence probes[14] fulfill some of these requirements; however, only a few probes[11,12,15,16] meet all these requirements. For example, Urano reported a Förster resonance energy transfer (FRET) strategy for the quantification of ultra-

State Key Laboratory of Coordination Chemistry, School of Chemistry and Chemical Engineering, Nanjing University, Nanjing, 210046, China. E-mail: zguo@nju.edu.cn; zshen@nju.edu.cn

† Electronic supplementary information (ESI) available. See DOI: 10.1039/d0sc02889d

‡ These authors contributed equally to this paper: Hanzhuang Liu and Wenting Song.

fast glutathione dynamics in the mitochondria based on an ultra-fast and reversible core reaction using the rhodamine platform.[11] Wang[12] and Yoon[16] reported excellent fluorescence probes based on Michael addition to α,β-unsaturated-ketone-derived coumarin for real-time quantification of intracellular GSH, respectively. Two significant advantages of using the Michael addition strategy are: (1) ratiometric fluorescence detection can be achieved with only one fluorescent molecule regardless of the FRET-related complications including spectral overlap, intermolecular distance, and spatial arrangement of the two molecules; and (2) due to the neutral nature of molecules, probes would uniformly distribute inside cells and monitor global GSH dynamics. However, this method could still be improved by the use of longer excitation wavelengths because high-energy blue lasers (405/450 nm) may cause significant damage on cells.

Taking the aforementioned factors into account, we synthesized a boron dipyrromethene (BODIPY)-based ratiometric fluorescence probe **1** (see Experimental section, Scheme 2) for real-time quantitative imaging of the dynamic changes in intracellular GSH levels. The probe exhibits rapid responses in both forward and reverse reactions with a wide response range toward GSH, covering the physiological GSH concentration, enabling a long period of real-time quantitative monitoring of intracellular GSH levels in response to cisplatin treatment. Using this probe allows a more comprehensive understanding of the relationship between GSH concentration and cisplatin-resistance of cells, which may assist help identify effective therapeutics for disease treatment (Scheme 1).

Results and discussion

Molecular design and spectroscopic properties in response to GSH

Our approach is based on the BODIPY fluorophore, which has excellent photo-physical properties, including strong absorption capacity and high fluorescence quantum yields.[17] Generally, the absorption and emission peaks of the classical BODIPY dye, *e.g.* 1,3,5,7-tetramethyl-8-phenyl-BODIPY appeared around

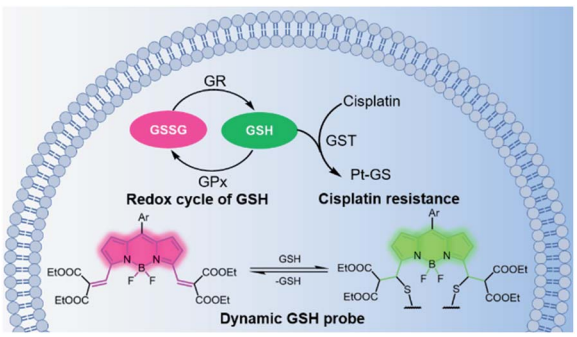

Scheme 1 Schematic diagram of GSH-related elimination of cisplatin and of real-time monitoring of the fluctuations in GSH levels using a reversible ratiometric probe **1** in living cells. GR: glutathione redutase, GPx: glutathione peroxidase, GST: glutathione-*S*-transferases, GSH: glutathione.

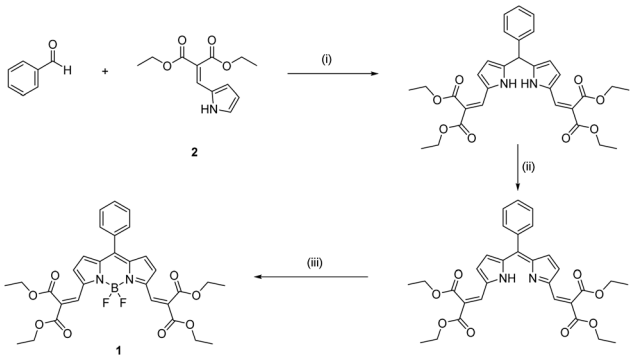

Scheme 2 Synthetic procedure of **1**: (i) TFA in CH_2Cl_2; (ii) DDQ; (iii) triethylamine and $BF_3 \cdot Et_2O$.

500 nm.[17] The electron-withdrawing diethyl malonate groups coupled through exocyclic double bonds at the 3,5-positions extends π-system delocalization and causes a red shift (from 500 to 600) in the absorption band compared to the tetramethyl BODIPY dyes.[17] The Michael addition of GSH to the vinyl group breaks the extension of the conjugated system, resulting in a *ca.* 68 nm blue-shift in the absorption and fluorescence bands and a significant colorimetric change from red to green (Fig. 1a and b). The spectroscopic properties of **1** were investigated by UV-vis absorption, and the emission spectra in 0.2 M phosphate-buffered saline (PBS, containing 30% ethanol) was obtained. Upon addition of GSH, both the absorption and fluorescence spectra exhibited rapid ratiometric responses. The absorption peak of **1** at 594 nm decreased, and a new peak at 527 nm emerged in conjunction with an apparent isosbestic point at 543 nm. The fluorescence peak at 613 nm decreased, and a new peak at 544 nm gradually increased with an apparent isosbestic point at 603 nm (Fig. S1 and S2†). Notably, the excitation wavelengths match the commercially available laser wavelengths (488, 514, and 543 nm), and the shift in emission profiles is large, making the probe suitable for two-channel ratiometric fluorescence imaging. Plotting the fluorescence intensity ratios at 544 nm ($\lambda_{ex} = 488$ nm) and 608 nm ($\lambda_{ex} = 543$ nm) as a function of GSH concentrations revealed a linear relationship ($R^2 = 0.9988$), covering the physiological GSH concentration range of 1–10 mM (Fig. 1c). The dissociation constant toward GSH K_d is 7.6 mM. To measure the rate and the reversibility of the reaction, we explored the time course of the fluorescence response of **1** toward variations in GSH levels. The probe exhibited rapid responses towards GSH concentrations in both forward and reverse reactions (Fig. 1d). The fluorescence intensity at 544 nm (F_{544}) was recorded to monitor the formation of **1**-GSH. Upon addition of different concentrations of GSH (2.5 mM, 5 mM, and 10 mM), F_{544} rapidly reached peak intensity. The calculated second order rate constant is 0.58 M^{-1} s^{-1}, which is 4 times as fast as that of TQ-Green,[7] used to quantify intracellular GSH concentration, but suffers from slow kinetics, making it difficult to monitor the intracellular GSH dynamics in real-time. The reverse reaction was monitored by following the decrease in intensity of F_{544}. GSH was depleted by adding *N*-ethylmaleimide (NEM) and increased again by adding GSH.

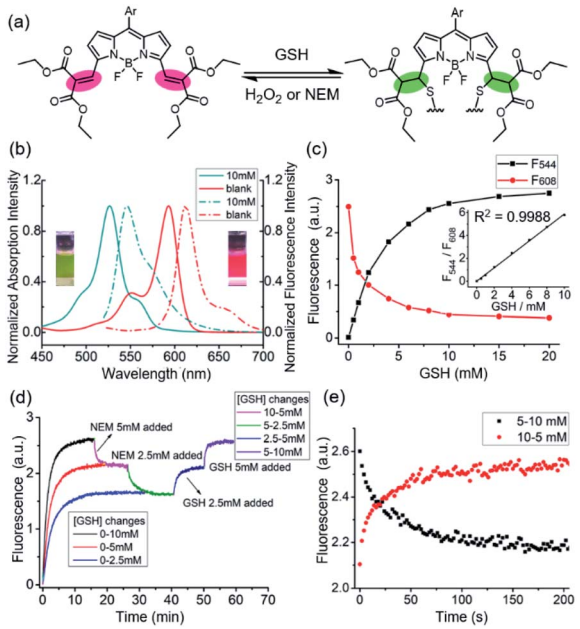

Fig. 1 Spectroscopic properties of **1** in response to GSH. (a) The reversible Michael addition reaction between **1** and GSH. (b) Absorption (solid line) and fluorescence (dash line) spectra of **1** (red) and **1**-GSH (dark cyan). (c) Dose-response curves of fluorescence intensity of **1** with increasing concentrations of GSH, excitation wavelengths are 560 nm and 488 nm for **1** and **1**+GSH, insert is the linear relationship between F_{544}/F_{608} and GSH concentrations. F_{544} (λ_{ex} = 488 nm) and F_{608} (λ_{ex} = 543 nm) are the fluorescence intensities for **1**-GSH and **1**, respectively. (d) Time-course fluorescence response of 1 toward variations of GSH. The formation of **1**-GSH and the reverse reaction was monitored by following the fluorescence intensity at 544 nm. GSH was depleted by adding *N*-ethylmaleimide (NEM) and increased by adding GSH. (e) Time-course fluorescence response spectra of **1** (10 μM) towards GSH concentration (5–10 mM) both in forward and reverse reactions in 0.2 M PBS (30% ethanol) at 37 °C. λ_{ex} = 488 nm, λ_{em} = 544 nm. GSH was depleted by adding *N*-ethylmaleimide (NEM). All data were recorded at 37 °C.

During GSH consumption and reperfusion, the change in fluorescence intensity closely matched the variation in GSH concentrations, thus supporting the highly reversible nature of the reaction between **1** and GSH. Moreover, **1** featured fast kinetics in both forward and reverse directions (Fig. 1d, e, S3 and S4†).

Selectivity and cytotoxicity

The selectivity of the Michael addition of a thiol-containing nucleophile to the fluorophore by other intracellular nucleophiles were next examined. Thiol-containing small molecules such as cysteine and homocysteine are known to have a signal comparable to that of GSH at millimolar concentration (Fig. S5 and S6†); however, their intracellular concentrations are less than 0.2 mM[18] and 0.01 mM,[19,20] respectively, and their interference should be negligible. The recorded F_{608}/F_{544} ratio is insensitive to amino-containing nucleophiles and other environmental factors within the physiological range,[11] including taurine, reactive oxygen, pH, and various amino acids (Fig. S7–S9†). Based on these results, **1** is suitable for selective monitoring of intracellular GSH, which is the most abundant thiol-containing nucleophile in living cells.

The cytotoxicity of **1** was determined by MTT assay. The cell viability was higher than 90% after incubation with 25 μM **1**, indicating that the probe has extremely low cytotoxicity at the applied concentration (Fig. S10†).

Reaction mechanism investigated by NMR

The reaction mechanism was investigated by ^{1}H-NMR and ^{13}C-NMR spectroscopy (Fig. 2 and S11–S14†) in $CDCl_3$. Since there were more protons on GSH and their signals could potentially obscure the vinylic proton signals of the probe, 2-mercaptoethanol (ME) was used to mimic GSH according to the literature.[9] Two-dimensional NMR spectra were obtained to aid signal assignments (Fig. S15–S19†). As shown in Fig. 2a and b, after the addition of ME, the vinylic proton signals at δ 8.24 ppm shifted significantly upfield to 3.98 ppm, and a new peak around 3.60 ppm was observed. The H–H COSY spectrum showed coupling between the peaks at 3.98 ppm and 3.60 ppm, and the peaks at 3.98 ppm appeared as doublet instead of triplet signals, which confirms that Michael addition has taken place at the double bonds at the 3,5-positions of BODIPY. The β-pyrrole protons shifted upfield from 6.92 and 6.81 to 6.73 and 6.31 ppm, suggesting that the π system of the indacene core was less extended after Michael addition. In the ^{13}C NMR spectrum (Fig. 2c and d), the two peaks at δ 129.54 ppm and 130.71 ppm corresponding to the sp^2 vinyl carbons at the 3,5-positions of BODIPY disappeared, while two new peaks assigned to the sp^3 carbons appeared at 51.32 ppm and 27.81 ppm. The double-bond carbons shifted for *ca.* 78–102 ppm upfield, while the chemical shifts of the other carbons were <10 ppm. These spectroscopic data verify that the reaction takes place at the double bonds at 3,5-positions of BODIPY through the Michael addition reaction by a thiol. The symmetrical ^{1}H-NMR and ^{13}C-NMR spectra suggest a bis-adduct was formed.

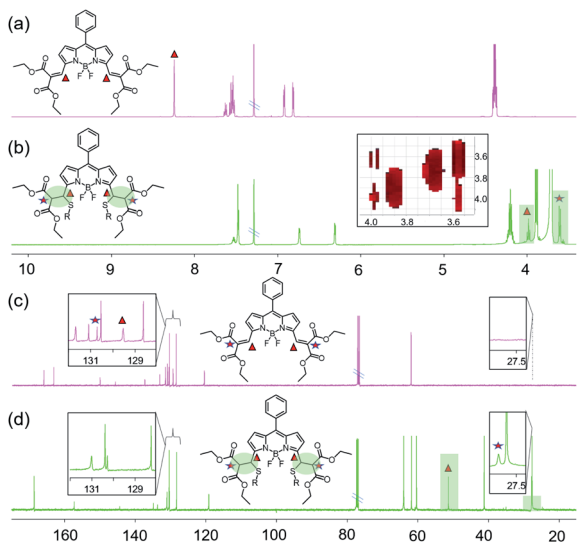

Fig. 2 ^{1}H and ^{13}C NMR of **1** and **1** + ME in $CDCl_3$. (a) ^{1}H NMR of **1**; (b) ^{1}H NMR of **1** + ME; (c) ^{13}C NMR of **1**; (d) ^{13}C NMR of **1** + ME.

Feasibility of real-time quantitative monitoring of GSH concentrations in living cells

HeLa cells were used to examine the suitability of **1** for real-time imaging and quantifying the changes in intracellular GSH concentrations in living cells (Fig. 3). The fluorescence images indicate that **1** was uniformly distributed in the cytosol with bright green and red fluorescence (Fig. 3a–c). Intracellular fluorescence was detected, and the fluorescence signal ratio was recorded and converted to GSH concentration by extrapolation based on a constructed calibration curve.[7,11] Plotting $(R - R_{min})/(R_{max} - R)$ as a function of GSH concentration, a reasonable linear calibration curve was then generated with $R^2 = 0.98$ (Fig. 3d), in which R is defined as the ratio of the fluorescence intensities between **1**-GSH and **1**, R_{min} and R_{max} correspond to the R values at zero and saturated GSH concentrations, respectively.[7] By employing this calibration curve, the intracellular GSH concentration was determined to be 3.9 ± 1.1 mM (Fig. 3e), which is similar to previously reported values,[7,11] and a cell lysate method revealed a GSH concentration of 4.2 ± 0.8 mM. The decrease in intracellular GSH concentration was induced by the addition of hydrogen peroxide (H_2O_2). The decrease in GSH levels is caused by the oxidation of GSH to GSSG as the cells scavenge H_2O_2, but it is replenished spontaneously by the reduction of the stored oxidized glutathione form (GSSG) to GSH in order to maintain the redox homeostasis in the cells. In line with this, the addition of H_2O_2 (1 mM) resulted in a 2.8 mM decrease in GSH concentration in 10 minutes, which was indicated by the reduced F_{green}/F_{red} ratio. Removal of the H_2O_2-containing media and restoration of normal medium led to a gradual recovery of the equilibrium GSH concentration in 40 minutes (Fig. 3f). These results show that **1** enables real-time quantitative monitoring of variations in GSH concentrations in living cells.

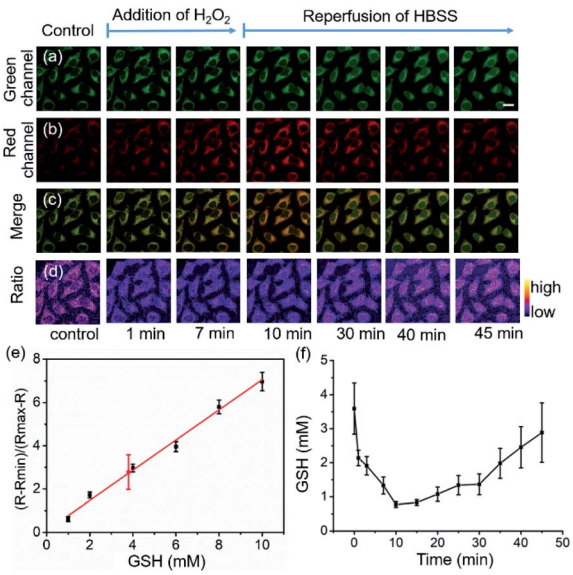

Fig. 3 Feasibility of real-time quantitative monitoring of GSH concentrations in living cells. For (a–d): Real-time GSH imaging with **1** (10 μM) in HeLa cells upon H_2O_2 (1 mM) treatment with a perfusion system. (a) Green channel; (b) red channel; (c) merge; (d) ratio image. (e) Standard curve of $(R - R_{min})/(R_{max} - R)$ as a function of GSH concentration under the same instrument setting as the live cell imaging experiment. R represents the fluorescence intensity ratio between 488 and 543 nm excitation; the data point in red represents the GSH concentration in HeLa cells based on statistical analyses of 11 cells. Error bars represent standard deviations. (f) Time course of GSH concentrations in HeLa cells upon H_2O_2 (1 mM) treatment. Mean values of GSH concentrations in individual cells ($n = 11$) were plotted, the error bars represent standard deviations. Scale bar, 10 μm. R is defined as the ratio of the fluorescence intensities between **1**-GSH and **1**, R_{min} and R_{max} correspond to the R values at zero and saturated GSH concentrations, respectively.

Real-time variations in intracellular GSH levels in response to platinum anticancer drugs

Having ascertained the feasibility of real-time quantitative monitoring of variations in GSH concentrations in living cells, we next monitored the real-time variations in intracellular GSH levels upon treatment with cisplatin anticancer drugs of drug-resistant A549-DDP cells and normal A549 cells (control). As shown in Fig. 4a–4c, in drug-resistant cells, GSH concentration increased rapidly in the early stages of drug treatment, and reached maximum in 350 min, indicating that the cells detoxify by producing large amounts of GSH rapidly through self-regulation. Then, the cellular GSH concentration fell to go back to the original level, indicating that the cells had completed the detoxification process. On the other hand, the concentration of GSH in normal A549 cells kept increasing until cell death, where no decline in GSH concentration was observed (Fig. S20†). Notably, these results reveal that the initial amount of GSH is not a crucial factor in cisplatin-resistance, which is consistent with the literature.[6] The rapid secretion of GSH did not prevent A549 apoptosis, which implies that cofactors may be required for GSH-mediated detoxification. One of the recognized mechanisms for cisplatin inactivation is the glutathione-*S*-transferase-catalyzed binding of GSH to cisplatin (Scheme 1).[3] Further studies are needed to confirm the mechanisms underlying the drug-resistance of the A549-DDP cells. The data presented here clearly show that the initial GSH concentration and the secretion speed are not fully responsible for cisplatin resistance. Whether the initial level or secretion rate of GSH is directly related to drug resistance of cancer cells is yet to be fully determined; however, our experiments indicate that the different trends in GSH fluctuations is crucial in distinguishing cisplatin-resistant from cisplatin-sensitive cells. While the cisplatin-sensitive A549 cells died with a high level of terminal GSH concentration, the drug-resistant A549-DDP cells survived with an arch bridge-shaped trend in GSH concentration. We have therefore shown that probe **1** is useful in monitoring real-time dynamic changes in cellular GSH concentrations during cisplatin treatment, which is significant in understanding the mechanism of drug resistance in living cells.

Since cancer cells have high rates of resistance to Pt^{II} complexes, Pt^{II} has a low therapeutic effect. Tetravalent platinum (Pt^{IV}) complexes as prodrugs have therefore increasingly attracted attention for cancer therapy. Pt^{IV} complexes have a low-spin, d^6 octahedral geometry, which makes it more bioavailable and less

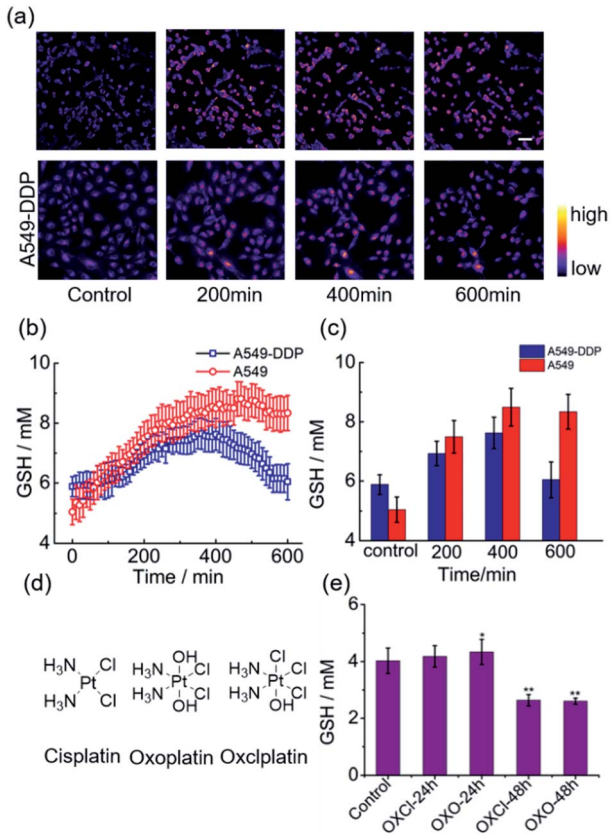

Fig. 4 Real-time variations in intracellular GSH levels in response to divalent platinum (Pt^{II}) and tetravalent platinum (Pt^{IV}) anticancer drugs. (a) Real-time ratiometric imaging of GSH in different timepoints. (b) Real-time average values of GSH concentration detected with **1** (10 μM) in A549 and A549-DDP cells upon cisplatin (10 μM) treatment (A549: $n = 77$; A549-DDP: $n = 86$). (c) Average GSH concentration detected with **1** (10 μM) in A549/A549-DDP cells upon cisplatin (10 μM) treatment in different timepoints (A549: $n = 77$; A549-DDP: $n = 86$). (d) Chemical structures of cisplatin, oxoplatin and oxclplatin; (e) average values of GSH concentration with **1** (10 μM) in A549 cells upon oxoplatin and oxclplatin (10 μM) treatment at different timepoints ($n = 15$). Scale bar, 50 μm. error bar represent s.d. *$p < 0.05$,**; $p < 0.01$.

toxic than Pt^{II} drugs, and it can be easily functionalized with other bioactive ligands to reduce the likelihood of developing drug resistance.[21] Previous studies have shown that GSH is involved in the reduction of Pt^{IV} prodrugs.[22] In this process, the Pt^{IV} prodrug is reduced to the cytotoxic Pt^{II} drug, and this process consumes GSH, thereby resulting in decreased GSH levels. In line with these speculations, we observed a significant decrease in GSH concentration in A549 cells after treatment with a Pt^{IV} prodrug for 48 h (Fig. 4e). Meanwhile, cell viability also declined after 48 h (Fig. S21†). This indicates that the reduction of the Pt^{IV} prodrug is accompanied by the decrease in GSH concentration, verifying that this reaction consumes GSH.

Experimental section

General synthesis of 1

1 was prepared *via* a conventional trifluoroacetic acid (TFA) catalyzed condensation reaction of benzaldehyde with pyrrole **2**, followed by oxidation with 2,3-dichloro-5,6-dicyano-1,4-benzoquinone (DDQ) and cyclization with $BF_3 \cdot Et_2O$ in a one-pot three steps process (Scheme 2). The structure of **1** was confirmed by ^1H NMR (Fig. S11†), ^{13}C NMR (Fig. S13†) and HRMS spectroscopy (Fig. S22 and S23†).

Synthetic details of 1

Benzaldehyde (2 mmol) and pyrrole **2** (2 mmol) were dissolved in dry dichloromethane (50 mL) under nitrogen, covered by aluminum foil. 100 μL TFA was added. Refluxing and stirring lasted for 24 to 72 hours until the pyrrole was completely consumed, as indicated by TLC. DDQ (2 mmol) was added, and the mixture was stirred for 30 minutes at room temperature. Triethylamine (3 mL) and boron trifluoride etherate (5–10 mL) were added. After 30 minutes of refluxing, the rose red solution was washed with water, saturated sodium bicarbonate solution, and then dried over anhydrous magnesium sulphate and concentrated under reduced pressure. Purification was undertaken by silica gel column chromatography using dichloromethane.

Steady-state absorption and fluorescence spectroscopy

Steady-state absorption and fluorescence measurements were carried out on Horiba Jobin Yvon spectrometer (Nanolog FL3-2iHR) and SHIMADZU UV-2550 spectrometer as well as HITACHI F4600 and Horiba Jobin-Yvon Fluoromax-4P fluorometers, employing UV-spectroscopic solvents. The temperature was kept constant at 298 ± 1 K except where noted. Dilute solutions with an absorbance of less than 1 at the absorption maximum were used for absorption measurements, and those less than 0.1 were used for fluorescence measurements. The latter were performed with a 90° standard geometry. Absolute fluorescence quantum yields were measured.

Determination of K_d value of 1 towards GSH[7,11]

The dissociation constant toward GSH K_d, was calculated according to eqn (1), in which R is defined as the ratio of the fluorescence intensities between **1**-GSH (544 nm) and the apparent fluorescence isosbestic point (603 nm), R_{min} and R_{max} correspond to the R values at zero and saturated GSH concentrations, respectively:

$$\frac{R - R_{min}}{R_{max} - R} = \frac{[GSH]}{K_d} \quad (1)$$

plotting $(R - R_{min})/(R_{max} - R)$ as a function of GSH concentration revealed a linear relationship ($R^2 = 0.9925$), the reciprocal of the slope affords the K_d as 7.6 mM (Fig. S24†).

Determination of reaction rate constant[7,11]

The reaction rate constant k was calculated according to the following eqn (2) and (3), in which $t_{1/2}$ is the half-life, k_{obs} denotes the pseudo-first-order kinetics:

$$t_{1/2} = \frac{\ln 2}{k_{obs}} = \frac{0.693}{k_{obs}} [s] \quad (2)$$

$$k = \frac{k_{obs}}{[GSH] + K_d}\left[M^{-1}\ s^{-1}\right] \quad (3)$$

$t_{1/2}$ was read from the time-course fluorescence spectrum (Fig. S4†) as 68 s, the concentration of GSH was 10 mM, then the rate constant k was calculated to be 0.58 M^{-1} s^{-1}.

Cell culture

HeLa cells were grown in DMEM media supplemented with 10% fetal bovine serum (FBS) and 1% 100 U mL^{-1}, 100 mg L^{-1} streptomycin in glass bottom dishes. Logarithmic growth cells were used for experiments. Cells were cultured under a controlled atmosphere (37 °C, 5% CO_2) for 24 h. The medium was removed and washed 3 times with HBSS then **1** (10 μM, dissolved in HBSS with 1% DMSO solubilization) was added and incubated for 30 min.

Real-time imaging of GSH in living cells

Confocal images were acquired with a confocal laser scanning microscopy (zeiss, LSM710). A 37 °C incubator was used during bioimaging. Confocal images were acquired with 488 nm laser/495–538 nm filter for green channel and 543 nm laser/590–700 nm filter for red channel. The gain values of the two channels are the same. All the microscope settings were kept consistent in each experiment.

Construction of calibration curve for confocal microscopy[7,11]

A calibration curve was constructed according to the previous reports[7,11] with slightly modification. Generally, GSH solutions (0–50 mM in PBS (containing 30% ethanol)) were prepared and mixed with compound **1** solution (10 μM final concentration). The above solutions were further mixed with a suspension containing 4.5 μm polystyrene beads. Fluorescence images were acquired with the same microscope settings adopted from prior experiments.

Software

Ratio images were constructed by Image J and Zeiss Zen 2008 software.

Construction of the GSH standard curve and quantification of intracellular GSH

A standard curve was constructed according to a procedure described in detail in ref. [3] A set of GSH solutions (0, 0.5, 1, 2, 6, 8, 10, 50 mM) in 0.1 M PBS/ethanol 7 : 3 (v/v) mixtures in the presence of 1 (10 μM final concentration) was prepared in 4-well glass bottom dishes. The above solutions were further mixed with a suspension containing 6.0 μm polystyrene beads. Fluorescence images were acquired with the same settings used for quantification imaging of GSH. The images were obtained by focusing the polystyrene beads. The imaging experiments were repeated twice, and three biological replicates were analysed for each imaging experiment. The mean values of the ratio were converted to GSH concentrations by using the obtained fitting curves according to the reference.

Quantification of GSH concentration using cell lysate assay

HeLa cells were seeded on a 100 mm dish and incubated in complete medium for 12 h. The cells were then collected in vials filled with protein extraction solution to release intracellular contents after counting cell number. After centrifugation for 10 min at 10 000×g and 4 °C, the collected lysate supernatant was collected. GSH quantification in the cell lysate was determined using an assay kit (Beyotime, S0053). The measurements were performed in triplicate.

Conclusions

In conclusion, we have developed a reversible ratiometric (red-*versus*-green) fluorescence probe for real-time quantitative imaging of GSH levels in living cells by taking advantage of a reversible Michael addition reaction of GSH with the vinyl-functionalized BODIPY dye. The probe displayed a wide response range toward GSH with a good linear relationship ($R^2 = 0.9988$) covering the physiological GSH concentration range (1–10 mM) and rapid responses in both forward and reverse reactions, which enables real-time monitoring of dynamic changes in intracellular GSH levels within 10 minutes. Combined with the advantages of the excitation wavelengths matched the commercial lasers (488, 514, and 543 nm), the large ratiometric shift of the emission peaks (64 nm), and the negligible cytotoxicity, real-time quantitative imaging of the intracellular GSH concentrations in response to cisplatin treatment can be performed continuously for 10 h. The arch bridge-shaped trend in GSH concentrations in the drug-resistant A549-DDP cells indicate that the cells underwent a detoxification process involving GSH. Taken together, the probe provides a useful tool for understanding the mechanisms underlying GSH-related cisplatin-resistance in cancer cells. In addition, the observation of a significant decrease in GSH concentration in A549 cells after treatment with a Pt^{IV} prodrug demonstrates that cellular GSH is involved in the reduction of Pt^{IV} to the cytotoxic Pt^{II} drug. Further studies are needed to correlate the dynamic fluctuations in intracellular GSH levels and the efficacy of Pt^{IV} prodrug in real-time. This study could inspire future designs of dynamic ratiometric fluorescence probes for real-time quantitative imaging of a wide range of biologically relevant species in order to precisely understand different pathophysiological processes.

Conflicts of interest

There are no conflicts to declare.

Acknowledgements

We would like to thank the National Natural Science Foundation of China (No. 21771102 to Z. S. and No. 21731004 to Z. G.) for the financial supports.

References

1 K. Xu, M. Qiang, W. Gao, R. Su, N. Li, Y. Gao, Y. Xie, F. Kong and B. Tang, *Chem. Sci.*, 2013, **4**, 1079.
2 K. Aquilano, S. Baldelli and M. R. Ciriolo, *Front. Pharmacol.*, 2014, **5**, 196.
3 X. Wang and Z. Guo, *Anti-Cancer Agents Med. Chem.*, 2007, **7**, 19–34.
4 A. K. Godwin, A. Meister, P. J. O'Dwyer, C. S. Huang, T. C. Hamilton and M. E. Anderson, *Proc. Natl. Acad. Sci. U. S. A.*, 1992, **89**, 3070–3074.
5 Y. Kasherman, S. Sturup and D. Gibson, *J. Med. Chem.*, 2009, **52**, 4319–4328.
6 Boubakari, K. Bracht, C. Neumann, R. Grünert and P. J. Bednarski, *Arch. Pharm.*, 2004, **337**, 668–671.
7 X. Jiang, Y. Yu, J. Chen, M. Zhao, H. Chen, X. Song, A. J. Matzuk, S. L. Carroll, X. Tan, A. Sizovs, N. Cheng, M. C. Wang and J. Wang, *ACS Chem. Biol.*, 2015, **10**, 864–874.
8 J. Chan, S. C. Dodani and C. J. Chang, *Nat. Chem.*, 2012, **4**, 973.
9 G.-J. Kim, K. Lee, H. Kwon and H.-J. Kim, *Org. Lett.*, 2011, **13**, 2799–2801.
10 R. Alford, H. M. Simpson, J. Duberman, G. C. Hill, M. Ogawa, C. Regino, H. Kobayashi and P. L. Choyke, *Mol. Imaging*, 2009, **8**(6), 341–354.
11 K. Umezawa, M. Yoshida, M. Kamiya, T. Yamasoba and Y. Urano, *Nat. Chem.*, 2016, **9**, 279–286.
12 X. Jiang, J. Chen, A. Bajic, C. Zhang, X. Song, S. L. Carroll, Z. L. Cai, M. Tang, M. Xue, N. Cheng, C. P. Schaaf, F. Li, K. R. MacKenzie, A. C. M. Ferreon, F. Xia, M. C. Wang, M. Maletic-Savatic and J. Wang, *Nat. Commun.*, 2017, **8**, 16087.
13 A. Kaur, J. L. Kolanowski and E. J. New, *Angew. Chem., Int. Ed.*, 2016, **55**, 1602–1613.
14 D. Lee, K. Jeong, X. Luo, G. Kim, Y. Yang, X. Chen, S. Kim and J. Yoon, *J. Mater. Chem. B*, 2018, **6**, 2541–2546.
15 X. Han, X. Song, F. Yu and L. Chen, *Chem. Sci.*, 2017, **8**, 6991–7002.
16 Z. Liu, X. Zhou, Y. Miao, Y. Hu, N. Kwon, X. Wu and J. Yoon, *Angew. Chem., Int. Ed.*, 2017, **56**, 5812–5816.
17 H. Lu, J. Mack, Y. Yang and Z. Shen, *Chem. Soc. Rev.*, 2014, **43**, 4778–4823.
18 S. Kenmoku, Y. Urano, H. Kojima and T. Nagano, *J. Am. Chem. Soc.*, 2007, **129**, 7313–7318.
19 S. Uno, M. Kamiya, T. Yoshihara, K. Sugawara, K. Okabe, M. C. Tarhan, H. Fujita, T. Funatsu, Y. Okada, S. Tobita and Y. Urano, *Nat. Chem.*, 2014, **6**, 681.
20 M. Sakabe, D. Asanuma, M. Kamiya, R. J. Iwatate, K. Hanaoka, T. Terai, T. Nagano and Y. Urano, *J. Am. Chem. Soc.*, 2013, **135**, 409–414.
21 D. Gibson, *J. Inorg. Biochem.*, 2019, **191**, 77–84.
22 Z. Zhu, Z. Wang, Y. Hao, C. Zhu, Y. Jiao, H. Chen, Y. M. Wang, J. Yan, Z. Guo and X. Wang, *Chem. Sci.*, 2016, **7**, 2864–2869.